GCOM–C1/SGLI Shadow index Algorithm Theoretical B asis Document

Masao Moriyama, Nagasaki University, Nagasaki, JAPAN.
Yoshiaki Honda, Koji Kajiwara, Chiba University, Chiba, Japan
Akiko Ono, Kindai University technical college, Japan

May 28, 2020

Contents

List of Figures

List of Tables

Chapter 1

Introduction

Almost all of the land cover has their own 3 dimentional structure, especially the vegetation, the shape of the canopy and the leaf is complicated so that the shaded area is depend on such kinds of 3 dimentional structure. For example Figure 1.1 shows the shaded area size difference correspondent to the canopy shape.

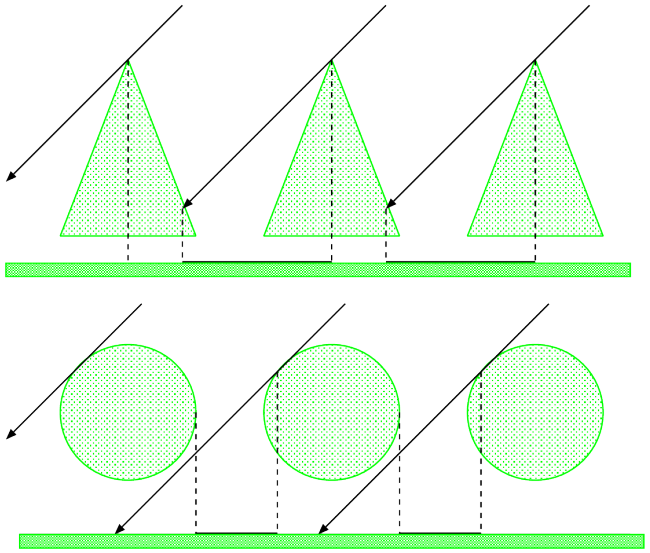

Figure 1.1: Schematic of the difference of the canopy shape and the shadow area

For the long term vegetation monitoring, such kind of shadow indormation shows the new aspect of the vegetation status such as the foliation, defoliation, felling and the species change and so on. So the SGLI provides the shadow index which shows the shadow content within a pixel as the new vegetation characteristic.

This document describes the definition and the data processing scheme of the shadow index and the validation scheme.

Chapter 2

Definition of Shadow Index

2.1 Surface reflectance scale up process

Within a pixel of the coarse spatial resolution (100 to 1000 [m]), there are many land cover with the various slope and aspect. the satellite observed radiance from such pixel I is the weighted mean of the radiance from the small segment I_s within a pixel. On the basis of this, the relationship between the reflectance of the segment and the average reflectance is clarified, this is called reflectance scale up.

For the scale up, the following assumption are made.

1. The i th. segment is the plane with the direct solar incident angle of θ'_{si} and has the area proportion is w_i and the constant reflectance ρ_i.
2. The direct and diffuse solar radiation incident to all segment within the pixel is constant.
3. The average of the direct and diffuse reflected radiance is the same as the direct and diffuse reflection part of the pixel.

The schematic of the scale up process is shown in Figure 2.1.

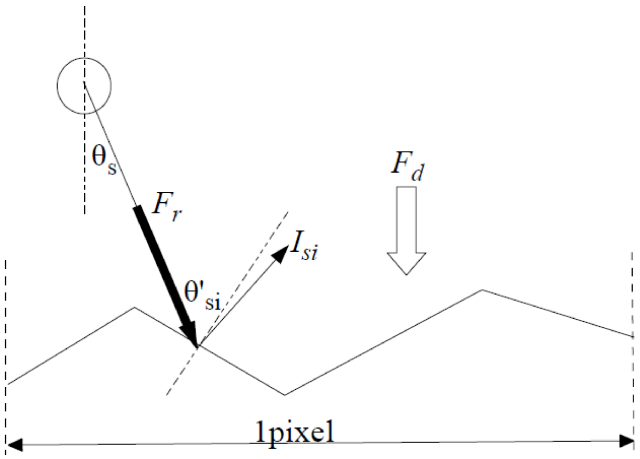

Figure 2.1: Schematic of reflectance scale up

The reflected radiance at the i segment $I-i$ can be expressed as Eq. (2.1),

$$I_{si} = (F_r \cos(\theta'_{si}) + F_d)\frac{\rho_i}{\pi}, \quad (\theta'_{si} > \pi/2, \cos(\theta'_{si}) = 0) \tag{2.1}$$

which F_r, F_d are the direct and diffuse solar irradiance respectively. The observed radiance of the pixel I is the weighted mean of the radiance from each segment $I-i$, and the area proportion of the segment w_i is the weight (*cf.* Eq. (2.2))

$$I_s = \sum_i w_i I_{si} = \sum_i w_i [(F_r \cos(\theta'_{si}) + F_d)\frac{\rho_i}{\pi}] \tag{2.2}$$

From the suumption 2, Eq. (2.3) can be deribed.

$$I_s = F_r \sum_i w_i \cos(\theta'_{si}) \frac{\rho_i}{\pi} + F_d \sum_i w_i \frac{\rho_i}{\pi} \tag{2.3}$$

The reflected radiance of the pixel I can be expressed as Eq. (2.4),

$$I_s = (F_r \cos(\theta'_s) + F_d) \frac{\bar{\rho}}{\pi} \tag{2.4}$$

where θ'_s and $\bar{\rho}$ are the average incident angle and the average reflectance of the pixel respectively. From Eq(2.3, 2.4), the average reflectance of the pixel can be the weighted mean of each segment reflectance with assumption 3 (*cf.* Eq. (2.5)) and the definition of the average indicent angle is expressed in Eq. (2.6).

$$\bar{\rho} = \sum_i w_i \rho_i \tag{2.5}$$

$$\sum_i w_i \cos(\theta'_{si}) \rho_i = \cos(\theta'_s) \bar{\rho} \tag{2.6}$$

2.2 Definition of Shadow Index

The satellite derived reflectance r is computed from the reflected radiance from the pixel with the apparent incident angle from the pixelwise elevation Θ'_s as Eq. (2.7).

$$r = \frac{\pi I_s}{F_r \cos(\Theta'_s) + F_d} \tag{2.7}$$

From the above discussion, Eq. (2.7) is expressed as Eq. (2.8).

$$r = \frac{F_r \cos(\theta'_s) + F_d}{F_r \cos(\Theta'_s) + F_d} \bar{\rho} \tag{2.8}$$

In the case of the diffuse irradiance is negligible such as SWIR spectrum, Eq. (2.8) is approximated as Eq. (2.9).

$$r = \frac{F_r \cos(\theta'_s)}{F_r \cos(\Theta'_s)} \bar{\rho} = \frac{\cos(\theta'_s)}{\cos(\Theta'_s)} \bar{\rho} \tag{2.9}$$

To clarify the shadow are proportion and the satellite derived reflectance, the numerical simulation of cosine of the average incident angle $\cos(\theta'_s) = \dfrac{\sum_i w_i \cos(\theta'_{si}) \rho_i}{\bar{\rho}}$ the under the condition described in Table 2.1 is made. In this simulation shadow area is defined as $\cos(\theta'_{si}) < 0$ case and compute the shadow are proportion.

Table 2.1: Simulation condition for the Shadow content simulation

ρ_i	Uniform random number within the range of 0 – 0.1, 0 – 0.3, 0 – 0.5, 0 – 0.7, 0 – 0.9
w_i	Uniform random number within the range of 1.0×10^{-10} – 1.0×10^{-6}
$1 - \cos(\theta'_{si})$	Log–normal distribution with the average of 0.1 – 0.9 and the standard deviation of 0.2, 0.4, 0.6 (*cf.* Figure2.2)
Cast shadow	Uniform random number within the range of 0 – 0.01, 0 – 0.05, 0 – 0.1

From the simulation result, it is clarified that the shadow area proportion can be expressed into the exponential of cosine of the average incident angle as shown in Figure 2.3.

The cosine of the average incident angle can be expressed from the apparent incident angle Θ'_s, the satellite derived reflectance r and the average reflectance $\bar{\rho}$ as Eq. (2.10) (*cf.* Eq. (2.9)).

$$\cos(\theta'_s) = \sum w_i \cos(\theta'_{si}) \frac{\rho_i}{\bar{\rho}} = \frac{r}{\bar{\rho}} \cos(\Theta'_s) \tag{2.10}$$

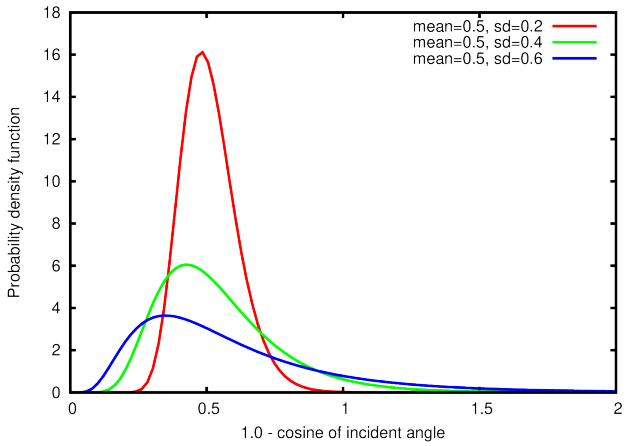

Figure 2.2: Log–normal distribution

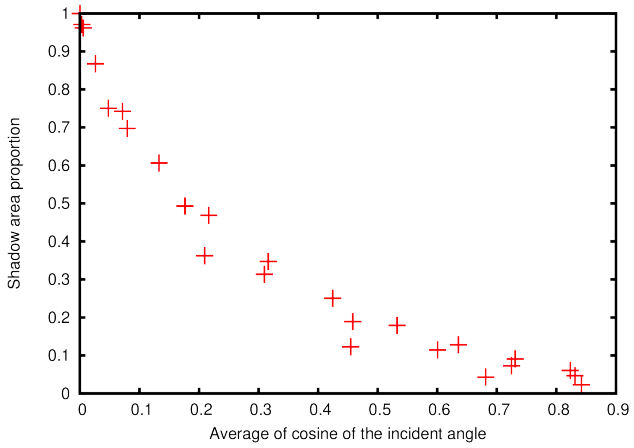

Figure 2.3: Relationship between the average of the cosine of the incident angle and the shadow area proportion

As the result, the Shadow Index (SI) which means the shadow area proportion within a pixel is defined as Eq. (2.11),

$$SI = a \exp\left[b \frac{r}{\bar{\rho}} \cos(\Theta'_s)\right] \tag{2.11}$$

where a and b are the regression coefficients.

Chapter 3

Operation

3.1 I/O dataset

SGLI Shadow Index (SI) is compted from the surface reflectance, in SGLI case the surface reflectance product is terrain corrected one. In this case the apparent incident angle Θ'_s in Eq. (2.7) which is computed from DEM is used. To compute SI, this incident angle is used as well as the SWIR reflectance (*cf.* Eq. (2.11)). For the finer spatial resolution, SGLI/SW3 (1.6[μm]) is used to compute SI. Also to notice the quality, the reflectance in red and near infrared spectrum, the land/water mask, the cloud mask and the solar and observation azimuth angle are used. The I/O dataset and processing flow are shown in Figure 3.1.

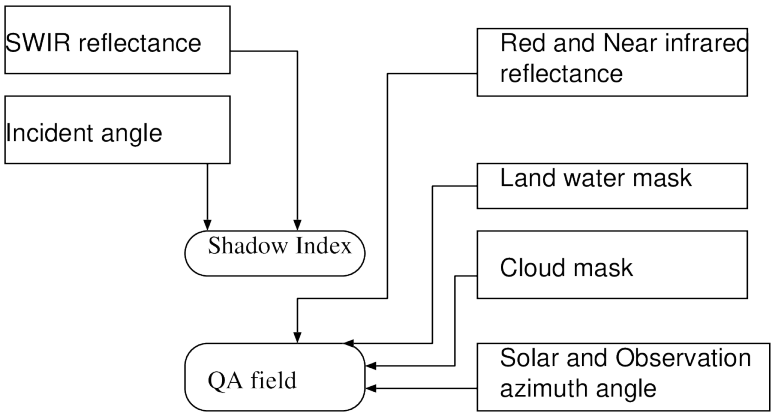

Figure 3.1: SI processing flow

The outputs of SGLI/SI product are SI field and QA field, both are 2 byte integer format. SI field contains the SI $\times$ 10000.

3.2 Quality Assurance

3.2.1 Concept

To notice the users about the quality of the product as well as the selection key of the spatial/temporal integration, the quality assurance (QA) field is necessary. In the SGLI case, The three vegetation related products NDVI and EVI and the shadow index are integrated into one hdf5 file named VGI. The QA plane of VGI is the mixup of the three vegetation related products' QA.

3.2.2 QA field bit assignment

SGLI/SI QA field has the 2 byte length and the bit assignment is shown in Table 3.1. SGLI/SI is the vegetation product, so that the extraction of the vegetation pixel is necessary. For this purpose, NDVI is used for the

thresholding. If NDVI vaue is smaller than the threshold, the bit 14 will be 1, this means the computed SI is not so correct because the average reflectance $\bar{\rho}$ in Eq. (2.11) is for the vegetation. SGLI/SI is affected by the solar and observation azimuth, in the case of the solar side observation, SI looks larger compated with in the case of the antisolar side observation especially in the regged terrain. Such observation direction is shown in the bit 15.

Table 3.1: Shadow index QA field (bit 15 is MSB)

Bit	Description	Bit	Description
00	no data	08	bad input for SWIR
01	land/water	09	band input for VNIR
02	mixed with land/water	10	Solar zenith is larger than 70[deg.]
03	Cloudy	11	sensor zenith angle is larger than 45[deg.]
04	Probably cloudy	12	EVI < -0.2 or EVI > 1.0
05	Snow or Ice	13	Large incident angle
06	No data for EVI	14	Small NDVI (< 0.65)
07	No data for SDI	15	Anti solar side

Chapter 4

Validation

4.1 Overview

Since the direct measurement of the shadow area proportion synchronous with the satellite observation is very difficult and limited to the small area, the high spatial resolution DSM (Digital Surface Model) which is generated at the same time or the same season of the satellite observation is applied for the shadow index validation. Such high spatial resolution DSM can be obtained from the 3 dimentional point cloud by LIDAR or SfM by UAV observation.

4.2 USGS 3DEP LIDAR point cloud based validation

USGS continues the high spatial resolution DSM generation project over the north american continent, it is called 3 dimentional elevation programme (3DEP). USGS opens the high spatial resolution LIDAR point cloud(LPC), its observation point interval is around 0.5 – 1 [m]. Based on the LPC, the following shadow index validation scheme is developed.

1. Generate the 1 [m] resolution DSM from the LPC throught the cubic spline interpolation.
2. Compute the direct solar irradiance at the same time as the satellite observation.
3. Identify the shadow which has no direct irradiance.
4. Average the shadow area within a SGLI pixel and compare the shadow index.

This validation flow is shown in Figure 4.1.

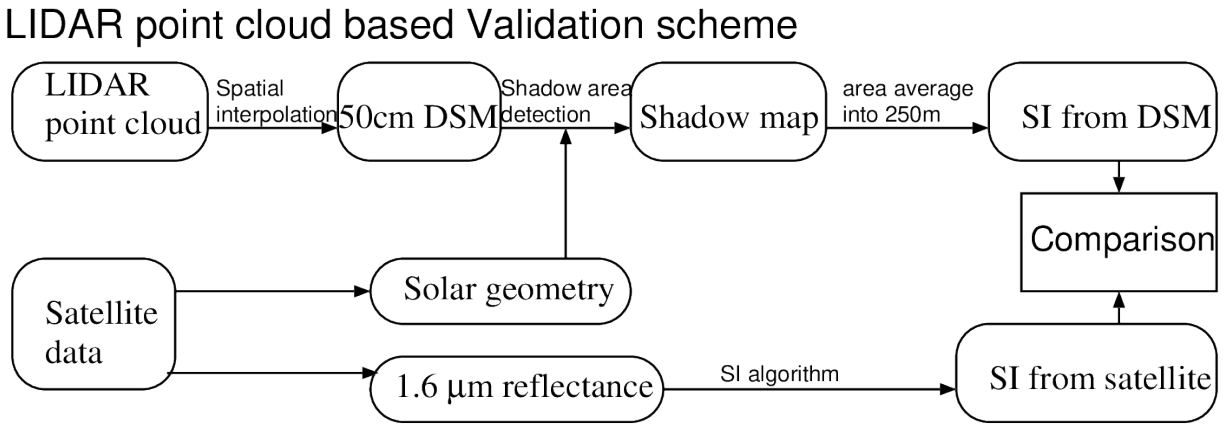

Figure 4.1: Shadow index validation flow

As an example, the truth data generation process based on the DSM around Modest, CA is shown in Figure 4.2.

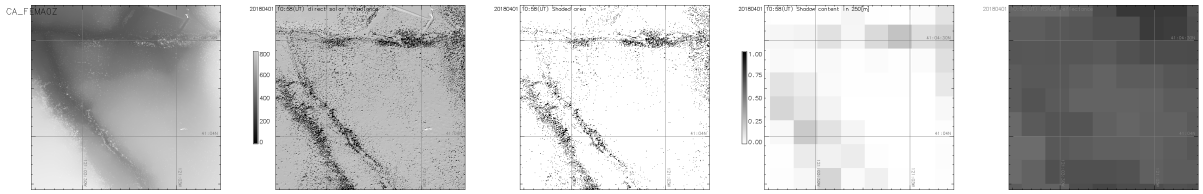

Figure 4.2: Shadow index truth data generation (from Left to Right: DSM, direct solar irradinace, shadow area, truth data and the shadow index computed from SGLI)

The validation will be made under the following condition to prevent the undesirable error contamination.

1. To avoid the size expanded pixel, satellite zenith is larger than 82 [deg.] (similar as LANDSAT observation geometry).
2. clear and non–cloud adjacent pixel.

On August 2018, the LIDAR observation near Modest, CA are made. From this LPC, SGLI shadow index validation is made on 16 June, 11 Oct. and 18 Nov., 2018. Also on July 2018, the LIDAR observation near Brighton, MI. are made. From this LPC, SGLI shadow index validation is made on 6 July and 23 Nov.. The comparison results are shown in Figure 4.3.

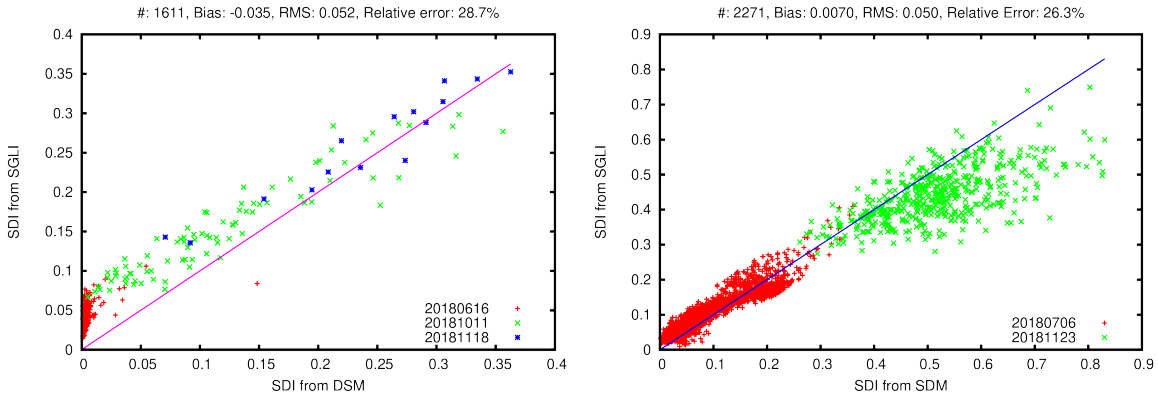

Figure 4.3: Comparison between DSM based and SGLI shadow index at Modest, CA. (Left) and Brighton, MI. (Right)

In both cases, the relative error of the shadow index estimation is less than 30 %, it satisfies the success criteria.